Hydrodeoxygenation of Refined Palm Kernel Oil Into Bioavtur Using Spray-Dry Impregnated Activated Carbon Supported-Mo Catalysts

Trisunaryanti, Wega
Faculty of Mathematics and Natural Sciences, Universitas Gadjah Mada

Triyono
Faculty of Mathematics and Natural Sciences, Universitas Gadjah Mada

Wijaya, Karna
Faculty of Mathematics and Natural Sciences, Universitas Gadjah Mada

Kartini, Indriana
Faculty of Mathematics and Natural Sciences, Universitas Gadjah Mada

他

https://doi.org/10.5109/7183322

出版情報：Evergreen. 11 (2), pp.652-664, 2024-06. 九州大学グリーンテクノロジー研究教育センター
バージョン：

Hydrodeoxygenation of Refined Palm Kernel Oil Into Bioavtur Using Spray-Dry Impregnated Activated Carbon Supported-Mo Catalysts

Wega Trisunaryanti[1*], Triyono[1], Karna Wijaya[1], Indriana Kartini[1], Suryo Purwono[2], Rodiansono[3], Ady Mara[4], Ike Ariska Dewi[1]

[1]Faculty of Mathematics and Natural Sciences, Universitas Gadjah Mada, Sekip Utara, 55281, Yogyakarta, Indonesia

[2] Faculty of Engineering, Universitas Gadjah Mada, Jl. Grafika No. 2, Senolowo, 55281, Yogyakarta, Indonesia

[3] Faculty of Mathematics and Natural Sciences, Universitas Lambung Mangkurat, JL A. Yani, Km. 35, 8, 70713, Kalimantan Selatan, Indonesia

[4] Department of Chemistry, Faculty of Mathematics and Natural Sciences, Universitas Sriwijaya, Jln. Pale mbang-Prabumulih KM 32 Indralaya, 30862 Sumatera Selatan, Indonesia

*Author to whom correspondence should be addressed:
E-mail: wegats@ugm.ac.id

(Received October 11, 2023; Revised April 21, 2024; Accepted April 24, 2024).

Abstract: The research was done to study the activity and selectivity of spray-dry Mo-impregnated catalysts on activated carbon for hydrodeoxygenation (HDO) of refined palm kernel oil (RPKO). This research was done by refining the palm kernel oil with degumming method. synthesizing Mo/C catalyst by impregnating ammonium heptamolybdate tetrahydrate ($(NH_4)_6Mo_7O_{24}\cdot 4H_2O$) onto activated carbon by spray-dry impregnation, calcinating, and then reducing. The HDO reaction was done on RPKO feed with Mo/C catalysts with H_2 gas flow. The catalyst was characterized using FT-IR, XRD, SEM-EDX, nitrogen desorption with Brunnauer-Emmet-Teller (BET) and Barrett-Joyner-Teller (BJH) equation, and NH_3-TPD. After HDO reaction using 3 different Mo/C catalysts, the 15-Mo/C catalyst had the highest acidity among catalysts containing Mo metal at 1.1472 mmol g^{-1}, catalyst area of 12.31 m^2 g^{-1} and a pore diameter of 6.13 nm. The 15-Mo/C catalyst produced liquid product conversion of 42.52wt%, with a bioavtur yield of 41.28wt%. The 5-Mo/C and 10-Mo/C catalysts produced liquid products of 35.40 and 38.35wt% with bioavtur yields of 33.48 and 36.09wt%, respectively. The 15-Mo/C catalyst had a promising performance during the second HDO run produced a liquid product of 36.11wt% and a bioavtur yield of 34.16wt% while the third run produced a liquid product conversion of 32.84wt% with a bioavtur yield of 31.24wt%.

Keywords: activated carbon; bioavtur; hydrodeoxygenation; molybdenum; refined palm kernel oil

1. Introduction

Along with the increasing population and the development of human activities in various sectors, demand for energy has become quite large. In this modern era, energy is an essential factor in production and a driving aspect of economic development around the world, but with less polluting solutions such as implementing carbon management, sustainable fuel and net zero emission by energy policy [1–6]. It is recorded that as much as 85% of current global energy needs still depend on fossil fuels, such as petroleum, coal, natural gas, and their derivatives[7]. Fossil fuels are a limited source of energy, so if their use continues to increase, their availability will be depleted[8,9]. The aviation sector is one of the sectors that is still dependent on fossil fuels. The development and expansion of the aviation sector are in line with its increasing consumption of fossil fuel-based aircraft. The increased use of fossil fuels has various impacts, one of which is on the environment. The impact of fossil fuel use on the environment includes the resulting emissions[10–12]. In 2018, it was stated that the aviation sector contributed 1.9% of greenhouse gas emissions and 2.5% of global CO_2 emissions[13]. To reduce the aviation sector's dependence on fossil fuels, the development of alternative fuels is

necessary.

Bioavtur is widely identified as an alternative to reduce fossil fuel dependence in the aviation sector[14]. Bioavtur can be produced by utilizing natural materials that are quite abundant and more environmentally friendly. The production of biofuel from plant-derived sources or natural materials is considered to have the potential to reduce greenhouse gas emissions. One of the natural materials that can be converted into bioavtur is vegetable oil, such as palm oil, canola oil, castor oil, and rapeseed oil[15]. Vegetable oils can be converted into bioavtur through a chemical reaction process. The conversion of vegetable oil into bioavtur fuel can be done through several types of processes, such as hydroprocessing, hydrotreating, deoxygenation, and cracking[16]. The advantage of using bioavtur is that the fuel is renewable and considered more environmentally friendly because it is produced from renewable sources such as vegetable oil[17,18].

Research by Yuki et al. from the EVERGREEN journal explained that, due to the oil crisis in the 1970s, many forms of research and development (R&D) pertaining to biomass utilization have been carried out in Japan[19]. Biomass has the potential to produce biofuels with renewable materials compared to the limited amount of fossil fuels. One of the vegetable oils that can be processed into bioavtur products is palm kernel oil (PKO). Many studies have been conducted related to the conversion of PKO into biological products. This is because PKO contains several compounds whose composition is like the compounds in bioavtur, which have carbon chains of C_7 to C_{16}[20]. Palm kernel oil (PKO) has a fatty acid content dominated by short-chain fatty acid compounds, such as lauric acid and myristic acid, which have 12 and 14 carbon chains, respectively[15]. The fatty acid content will be converted into bioavtur through the hydrodeoxygenation (HDO) reaction.

The catalyst must be able to function as Brønsted acid sites to enhance the frequency of HDO reactions. These sites play an important role in HDO reactions because they can bind hydrogen and then release it to interact with the hydrodeoxygenated vegetable oil[21,22]. Noble metal catalysts, such as Pd and Pt metals, are widely used in the process of converting vegetable oil through deoxygenation reactions[23]. This is because the use of noble metal catalysts generally results in a high product conversion rate[24,25]. However, noble metal catalysts have disadvantages such as their relatively expensive price and limited availability in nature[26]. Therefore, noble metals are less favourable for bioavtur production catalysts, especially on an industrial scale.

Transition metals are one of the alternatives that can be used as catalysts to replace precious metals. Transition metals are generally quite abundant and relatively cheaper[27]. Molybdenum (Mo) metal is one of the transition metals that has been widely studied and applied as a catalyst in deoxygenation reactions. Because Mo metal functions as a Brønsted acid side that may activate C–O, it plays a part in deoxygenation processes. Due to its single electron in the d orbital that acts as a homolytic Brønsted acid and its empty p orbital that acts as a Lewis acid that binds hydrogen, Mo metal can be used as an HDO catalyst. Mo metal is a stable electron metal due to its half-full d orbital[28–30].

An EVERGREEN journal article by Nugrahaningtyas et al. produced gasoline from oleic acid using CoMo metal catalyst[31]. This shows that Mo metal is proven to have good activity and to convert vegetable oils into hydrocarbon products. Therefore, the use of Mo metal in HDO reactions supports selectivity towards deoxygenated products[23,31].

Other than the metal used as a catalyst for the HDO reaction, the support for the catalyst is essential. The support is needed as a surface for the metal while maximizing the performance of the catalyst. The material needs to be considered in several aspects, such as acidity and porosity. During the HDO reaction, the acidity of the support material can affect the course of the reaction. The acidity of the support can result in high product conversion, but the durability of the catalyst life becomes low or easily deactivated[26]. A study by Wiratini et al. from Evergreen shows that carbon has potential as a catalyst and support from its surface area, chemical inertness, and porosity, resulting in a higher reaction rate[32]. Activated carbon is one of the materials that can be used as a support because of its adequate acidity, large surface area, and porosity. Activated carbon can also be produced from waste and then applied. For example, taken from the EVERGREEN journal, activated carbon was applied as vehicle exhaust gas by Yusuf et al.[33], water vapor adsorption by Ridassepri et al.[34], and fuel cell catalyst support by Fadlilatul et al.[35]. Activated carbon is also considered quite resistant to acidity changes, high temperatures, and pressures. Activated carbon can be synthesized from waste or biomass, so the price is relatively cheaper, and the availability is quite abundant. Activated carbon has carboxylic functional groups that can act as Bronsted acid sites, which are also needed in HDO reactions.

The method that can be used for the synthesis of catalyst material is the impregnation method. Impregnation is the process of dispersing metals onto the support[36]. Impregnation methods are generally divided into wet impregnation and dry impregnation. Wet impregnation is a method that is generally more widely used because it is considered effective for dispersing active metals through their precursor salts[37]. Wet impregnation is done by immersing the support into an excess metal solution and then calcining the catalyst. However, in industry, the conventional wet impregnation method by immersion becomes ineffective because it requires a lot of time and cost and produces unnecessary waste. Dry impregnation with the spray method has the advantage of controlling the production of uniformly sized

particles and distributing them uniformly throughout the catalyst surface. Spray-dry impregnation can minimize the need for solvents and shorten the catalyst's drying period[38,39]. Water treatment, ethanol dehydration, and catalyst production were done using the spray approach [40–42].

Therefore, in this study, catalyst synthesis was carried out by the dry impregnation method by spray, which has the novelty that spray-dry impregnation for hydrocracking catalyst is not yet widely developed. Therefore, in this study, the synthesis of Mo metal catalyst embedded in activated carbon material (Mo/C) using dry impregnation by spray as HDO catalyst for RPKO feed into bioavtur was carried out.

2. Materials and Methods

2.1 Materials

Activated carbon, Palm Kernel Oil (PKO) produced by PT Sinar Mas, ammonium heptamolybdate tetrahydrate ($(NH_4)_6Mo_7O_{24}$-$4H_2O$, Sigma-Aldrich), deionized water, bentonite, and 85% H_3PO_4 solution were produced from CV Bima Aksara Nusa.

2.2 Refined Palm Kernel Oil (RPKO) Preparation

The refining of RPKO was done by heating 500 mL of PKO to a temperature of 90 °C in a beaker glass, stirring with a magnetic stirrer, and adding an 85% H_3PO_4 solution, as much as 0.05 mL per 100 mL of oil for 10 min. After that, the oil was cooled down, and then centrifuged for 30 min at 2500 rpm using Kokusan H-107 centrifuge. The oil was filtered from the gum using vacuum filtration using vacuum flask, buchner funnel, and filter paper. The degummed PKO was added with bentonite, as much as 3% of the PKO volume. The PKO was then refluxed at 105 °C, stirred for 2 h, and then centrifuged for 30 min at 2500 rpm using a Kokusan H-107 centrifuge and refined palm kernel oil (RPKO) was obtained. The RPKO was derivatized by esterification using methanol and then characterized using a gas chromatography-mass spectrometer (GC-MS, Shimadzu QP2010S).

2.3 Preparation of Mo/C catalyst

The Mo/C catalyst was prepared by the dry impregnation method by spraying the metal precursor which is aqueous tetrahydrate salt ($(NH_4)_6Mo_7O_{24}$-$4H_2O$). The catalyst was prepared by varying the Mo metal content, which was 5, 10, and 15wt% of the activated carbon. For each catalyst, the $(NH_4)_6Mo_7O_{24}$-$4H_2O$ was dissolved in deionized water and sprayed on the activated carbon using a spray bottle, then mixed using a mortar and pestle until it formed a paste texture. The paste was dried using an oven at 110 °C for 2 h. After dried using an oven, the catalyst was calcinated using N_2 gas at 500 °C in a furnace with a gas flow rate of 10 mL min^{-1} for 5 h and then reduced by H_2 gas flow with a gas flow rate of 10 mL min^{-1} at 500 °C for 5 h. Following the preparation, each catalyst was named according to its Mo metal content, which was 5-Mo/C, 10-Mo/C, and 15-Mo/C.

2.4 Characterization of Mo/C Catalysts

The activated carbon, 5-Mo/C, 10-Mo/C, and 15-Mo/C catalysts were characterized for functional group analysis using Fourier Transform Infrared Spectroscopy (FTIR, Shimadzu IR Prestige-21), crystalinity using X-Ray Diffraction (XRD, Shimadzu XRD-6000), surface by using nitrogen desorption with Brunnauer-Emmet-Teller (BET) and Barrett-Joyner-Teller (BJH) equation (Quantachrome TouchWin v1.22) with 1 h and 300 °C degassing time and temperature, morphology and metal content using Scanning Electron Microscope-Energy Dispersive X-Ray (SEM-EDX, JEOL JED-2300), and acidity by using Temperature Programmed Desorption of Ammonia (NH_3-TPD, Micromeritrics Chemisorb 2750).

2.5 Catalytic Activity Test

The catalytic activity test was conducted through the HDO process with RPKO feed in a semi-batch stainless steel reactor with a double furnace in a one-pot system. The HDO process was carried out with no catalyst (thermal cracking), activated carbon, and Mo/C catalyst variants. The catalyst-to-feed ratio was set to 1:200 (w/v). The HDO process was done at a temperature between 400 and 600 °C and flowed with H_2 gas at a flow rate of 10 mL min^{-1} for 2 h. The resulting liquid product was separated into two fractions, which were at 400–500 °C and 500–600 °C. The most liquid-producing catalyst was used for the usability test by running HDO three times. The liquid products were characterized using GC-MS, and the catalyst was characterized using SEM-EDX after three HDO runs. The HDO product fractions were calculated from Eq. 1 to Eq. 4, where A_B is the GC area of bioavtur compounds, A_n is the GC area of non-bioavtur compounds, Ao is the GC area of oxygenated compounds, and A_{total} is the total GC area. The W_{LP} and W_F are HDO liquid product weight and RPKO feed weight:

$$Liquid\ Product\ (wt\%) = \frac{W_{LP}}{W_F} \times 100\% \quad (1)$$

$$Y_{BA}\ (\text{wt\%}) = \frac{A_B}{A_{total}} \times \frac{W_{LP}}{W_F} \times 100\% \quad (2)$$

$$Y_{NB}\ (\text{wt\%}) = \frac{A_n}{A_{total}} \times \frac{W_{LP}}{W_F} \times 100\% \quad (3)$$

$$Y_{OC}\ (\text{wt\%}) = \frac{A_o}{A_{total}} \times \frac{W_{LP}}{W_F} \times 100\% \quad (4)$$

3. Results and Discussion

3.1 Characterization of RPKO

The characterization of RPKO using GCMS was shown in Table 1.

Table 1. Compounds of RPKO using GC-MS.

Retention Time	SI	GC Area (%)	Compound	
			Formula	Name
6.824	96	0.2	$C_6H_{12}O_2$	Caproic acid
13.674	97	4.1	$C_7H_{14}O_2$	Caprylic acid
20.097	95	4.08	$C_{10}H_{20}O_2$	Capric acid
25.772	94	54.7	$C_{12}O_{24}O_2$	Lauric acid
30.689	96	16.27	$C_{14}H_{28}O_2$	Myristic acid
35.147	95	6.95	$C_{16}H_{32}O_2$	Palmitic acid
38.582	94	1.34	$C_{16}H_{30}O_2$	9,12-hexadecadienic acid
38.731	96	10.68	$C_{18}H_{34}O_2$	Oleic acid
39.208	96	1.67	$C_{18}H_{38}O_2$	Stearic acid

Based on the results of the GC-MS analysis in Table 1, the main content in RPKO is dominated by lauric acid and myristic acid compounds of 54.70 and 16.27%, respectively. The RPKO should mostly contain triglycerides, but the result shows carboxylic acids because GCMS needs volatile compounds to be detected; thus, the RPKO underwent a derivation process by esterification using methanol. The characterization used a DB-5MS column with a GC oven at 70 ºC. Lauric and myristic acids are in the bioavtur range (C_7–C_{16}), which means bioavtur can be produced by the HDO reaction of RPKO.

3.2 Catalyst Functional Group Characterization

The activated carbon, 5-Mo/C, 10-Mo/C, and 15-Mo/C were characterized using FT-IR spectra and the result was shown in Fig. 1 and Table 2.

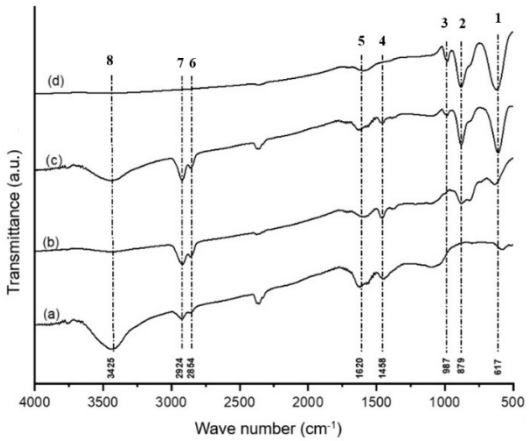

Fig. 1: FT-IR spectra of: (a) Activated carbon, (b) 5-Mo/C, (c) 10-Mo/C, and (d) 15-Mo/C catalysts.

Table 2. FT-IR spectra interpretation of activated carbon, 5-Mo/C, 10-Mo/C, and 15-Mo/C catalysts.

No.	Wavenumber (cm^{-1})				Bond type and vibration	Ref.
	Activated carbon	5-Mo/C	10-Mo/C	15-Mo/C		
1	-	617	617	617	O-Mo-O (Bending)	[43]
2	-	879	879	879	Mo=O	[43]
3	-	-	987	987	Mo-O-Mo (stretching)	[43]
4	1458	1458	1458	-	C=C (stretching)	[44]
5	1620	1620	1620	1620	C=O (stretching)	[44]
6	2854	2854	2854	-	C-H (symmetrical stretching)	[44]
7	2924	2924	2924	-	C-H (asymmetrical stretching)	[44]
8	3425	-	3425	-	-OH	[44]

Based on the analysis, the IR spectra display bands derived from metal-oxygen bonds and bands derived from the activated carbon, as shown in Fig. 1 and Table 2. The vibrations from the functional groups have different characteristics. The bending vibration has the atoms moving at an angle along the bond axis, resulting in a different bond angle. As for stretching, a bonded molecule goes towards and away from the centre atom, resulting in different bond lengths. Symmetrical stretching means the stretching was done where two atoms moved into and away from the centre atom at the same time, while asymmetrical stretching has one atom move away from the centre atom and the other atom move into the center atom. Peaks related to the presence of activated carbon are shown in several peaks, such as peaks at wave numbers

1458, 1620, 2854, 2924, and 3425 cm^{-1}. The peaks at wave numbers around 617, 879, and 987 cm^{-1} belong to the Mo metal bonded with oxygen. It shows the successful impregnation of Mo metal onto the activated carbon in all variations.

3.3 Catalyst Crystallinity and Minerals Characterization

Crystallinity and minerals of activated carbon, 5-Mo/C, 10-Mo/C, and 15-Mo/C were characterized using XRD and showed in Fig. 2 and Table 3.

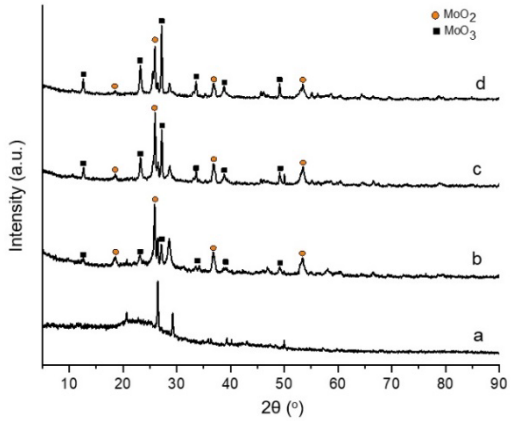

Fig. 2: Diffractogram of: (a) Activated carbon, (b) 5-Mo/C, (c) 10-Mo/C, and (d) 15-Mo/C catalysts.

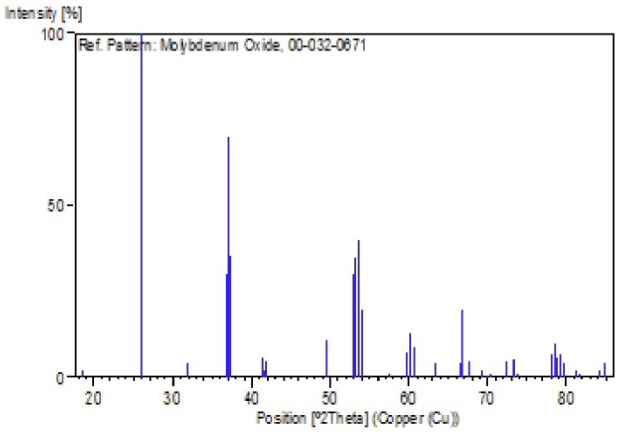

Fig. 3: Diffractogram of MoO_2 from JCPDS (ICDD) database

Based on Fig. 2 that was made using OriginPro software, the analysis shows matching XRD peaks with mordenite minerals using the JCPDS (ICDD) database, which are MoO_2 species with a monoclinic crystal system (JCPDS 032-0671), which is shown in Fig. 3, and MoO_3 species with an orthorhombic crystal system (JCPDS 005-0508) but have no diffractogram. The diffraction peaks of MoO2 appear at 2θ of 18.5, 25.9, 36.8, and 53.5˚ with diffraction planes of (-101), (-111), (111), and (-312), respectively. The MoO_3 diffraction peaks appeared at 2θ of 12.6, 23.2, 27.2, 33.6, 38.8, and 49.1˚ with diffraction planes of (020), (110), (021), (111), (060), and (002), respectively. The peaks formed are quite sharp, indicating that the catalysts have good crystallinity[45]. The diffractogram pattern in Fig. 2 for activated carbon catalyst (C) has a wide peak, indicating that the material is amorphous. The 5-Mo/C, 10-Mo/C, and 15-Mo/C catalysts show sharp crystal peaks.

Catalyst reduction in the catalyst synthesis process has the main purpose of obtaining Mo species with an oxidation number of 0. The appearance of MoO_2 and MoO_3 in the catalyst sample indicates that the catalyst reduction process has not taken place completely. According to Hossain et al.[46], in their research, Mo is indeed very difficult to reduce to its metal form. However, several studies found that Mo metal catalysts in their oxide form, such as MoO_2 and MoO_3, also have catalytic activity towards HDO reactions.

Table 3. Degree of crystallinity of of activated carbon, 5-Mo/C, 10-Mo/C, and 15-Mo/C catalysts.

Sample	Degree of crystallinity (%)
Activated Carbon	0.00
5-Mo/C	48.45
10-Mo/C	50.87
15-Mo/C	54.97

The crystallinity of each catalyst was determined by dividing the peak areas by the total area from the XRD data using Origin Pro software using the equation below:

$$Crystallinity = \frac{A_{peak}}{A_{total}} \quad (5)$$

Based on Table 3, the presence of Mo metal impregnated into the activated carbon material causes changes in the amorphous structure of the activated carbon into a crystalline structure. The crystallinity of the catalyst increases as the Mo metal added increases. This shows that metal impregnation on activated carbon caused an increase in crystallinity in the catalyst. The presence of molybdenum as an active metal tends to form a crystalline structure on the catalyst.

3.4 Catalyst Morphology and Composition Characterization

SEM-EDX was used to characterized morphology and composition of the respective catalysts. The result was shown in Fig. 4, Table 4, and Fig. 5.

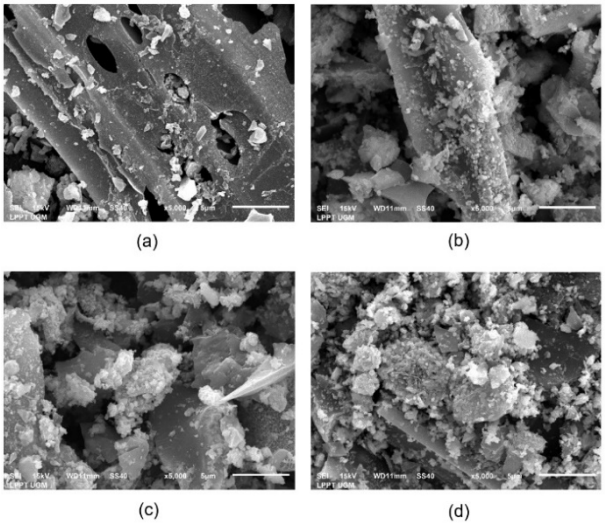

Fig.4: Morphology of: (a) Activated carbon, (b) 5-Mo/C, (c) 10-Mo/C, and (d) 15-Mo/C catalysts using SEM image.

Based on Fig. 4, catalyst C, which is activated carbon, has a smooth morphology, and has a solid sheet-like structure in the form of a solid and long strip. After metal impregnation into activated carbon, the morphology-impregnated catalyst forms a kind of lump. Although there are still parts of the surface that look smooth, the morphology of the catalyst is no longer in the form of thin sheets like before Mo metal impregnation. This indicates that metal impregnation affects the shape and morphology of the catalyst surface.

Table 4 Elemental composition of activated carbon, 5-Mo/C, 10-Mo/C, and 15-Mo/C catalysts using EDX analysis.

Element	Composition (wt%)			
	Activated carbon	5-Mo/C	10-Mo/C	15-Mo/C
Mo	-	10.81	20.68	29.75
C	77.58	66.78	44.21	47.50
O	19.36	20.27	21.48	21.91
Al	0.59	-	-	-
Si	0.70	0.20	0.45	-
K	0.40	0.45	0.22	0.26
Ca	1.37	0.86	0.56	0.57
Impurities	-	0.64	12.4	-

Based on Table 4, as the amount of Mo metal impregnated increases, the abundance of Mo elements in the catalyst material also increases. The composition of carbon elements gradually decreases with an increase in the amount of Mo metal. This is possible because the inclusion of more Mo metal causes the percentage of carbon atoms in activated carbon to decrease. The abundance of oxygen also increased along with the increase in molecular weight. The increased oxygen is likely to come from molybdenum oxide. The data is supported by the results of the XRD analysis in Fig. 2, where the compound found in the catalyst material is molybdenum in its oxide form. Table 4 also shows that there are some elements that disappear after the synthesis process, such as Si and Al. This event can be possible due to the preparation of the catalyst during the calcination or reduction process. The Mo metal content is higher than the added amount because the surface distribution is not even. The spray-dry impregnation method used a spray bottle, manual grinding using a mortar and pestle, and stirring with no exact duration.

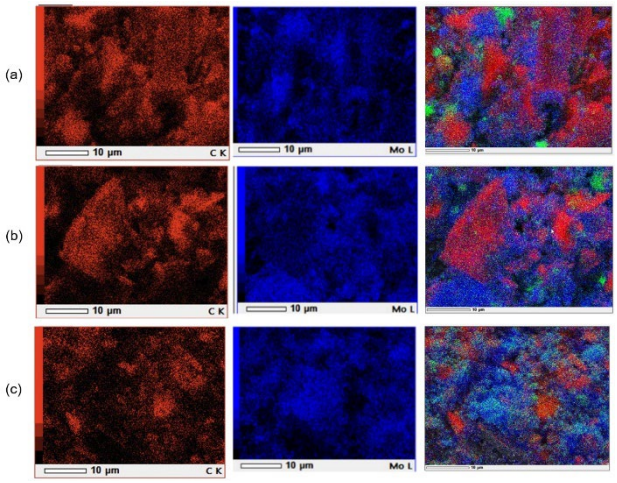

Fig. 5: Carbon and Molybdenum mapping of: (a) 5-Mo/C, (b) 10-Mo/C, and (c) 15-Mo/C catalysts using SEM-EDX.

The SEM-EDX mapping of each catalyst is shown in Fig. 5. As shown in Fig. 5, the blue color shows the species of the element Mo, and the red color shows the species of the element C. Based on the results of the mapping, Mo metal has been successfully impregnated on the surface of the catalyst, but there is still agglomeration at some point. Mapping results also show that the higher the concentration of Mo metal that is impregnated into activated carbon, the more metal that covers the surface of activated carbon. In the 5-Mo/C and 10-Mo/C catalysts, the distribution of Mo metal is still not evenly distributed, and agglomeration occurs in some parts of the catalyst. The 15-Mo/C catalyst showed that the Mo metal was more evenly distributed, but agglomerations were still formed. Metal distribution on the surface of the carrier greatly affects the catalytic activity of the catalyst. Evenly distributed metal particles will show an increasingly even distribution of active sites on the surface of the carrier. The active sites formed will increase the activity and selectivity of the catalyst for the HDO reaction in RPKO[47].

3.5 Catalyst Surface Porosity Characterization

Catalysts porosity and surface were characterized using Nitrogen desorption with Brunnauer-Emmet-Teller (BET) equation for the surface area and Barrett-Joyner-Teller (BJH) equation for the pore volume and diameter distribution. The result was shown in Table 5, Fig. 6, and Fig. 7.

Table 5. Surface characters of activated carbon, 5-Mo/C, 10-Mo/C, and 15-Mo/C catalysts.

Sample	Surface area (m^2 g^{-1})	Pore volume (cm^3 g^{-1})	Pore diameter (nm)
C	71.39	0.062	3.48
5-Mo/C	22.09	0.028	5.09
10-Mo/C	8.27	0.012	6.03
15-Mo/C	12.31	0.019	6.13

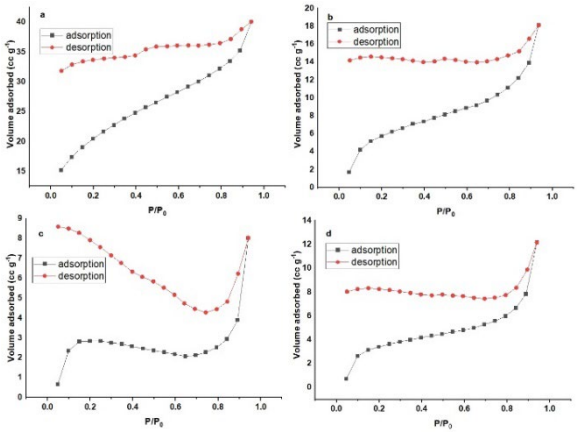

Fig. 6: Isotherm profile of: (a) activated carbon, (b) 5-Mo/C, (c) 10-Mo/C, and (d) 15-Mo/C catalysts using BJH Equation

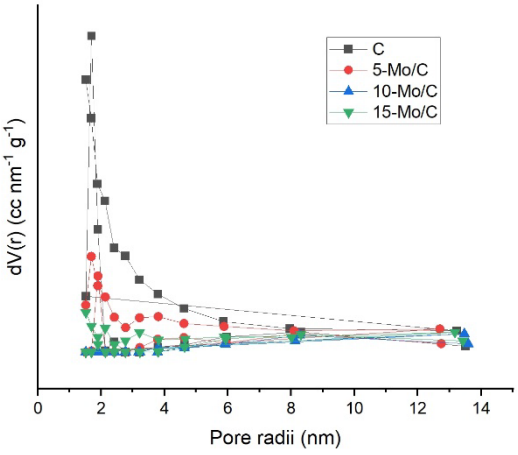

Fig. 7: Pore size distribution of activated carbon (C), 5-Mo/C, 10-Mo/C, and 15-Mo/C catalysts using BJH Equation

The area and pore volume of the catalyst support in Table 5 decreased after the Mo metal impregnation. Molybdenum metal blocked the pores on the activated carbon. As the concentration of Mo metal increases, the diameter of the pores increases. Many small pores are covered by molybdenum and leave large pores. A larger surface area results in more frequent catalytic activity from increased interaction between the feed and the active sites of the catalyst support. As for the isotherm profile and pore size distribution in Figs. 6 and 7, the results are not ideal. This may be because the degassing temperature needs to be higher, and the degassing time is not long enough, although it has been degassed for 24 hours. The catalyst material has a pore size distribution, which is shown by the pore radius distribution curve in Fig. 7. Based on the radius distribution curve in Fig. 7, it shows the pore size distribution of the catalyst materials C, 5-Mo/C, 10-Mo/C, and 15-Mo/C is dominated by the pore radius, which is predominantly distributed at a size of 2-4 nm. This proves that the Mo catalyst material embedded in activated carbon has a mesoporous size.

3.6 Catalyst Acidity Characterization

The NH_3-TPD analysis result was shown in Fig. 8. And Table 6.

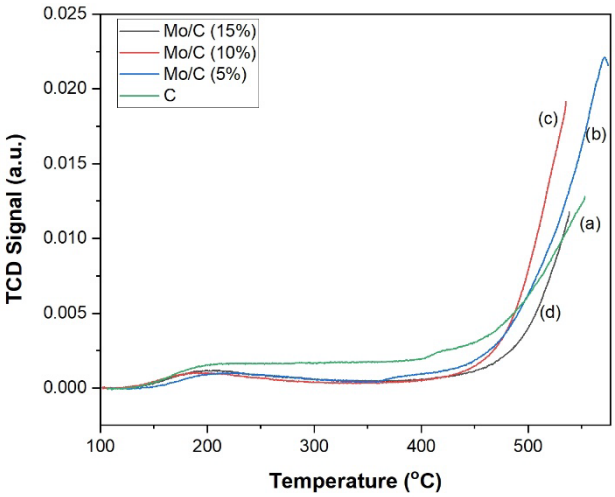

Fig. 8 Analysis curve of: (a) Activated carbon, (b) 5-Mo/C, (c) 10-Mo/C, and (d) 15-Mo/C catalysts using OriginPro software.

Table 6. Acidity of activated carbon, 5-Mo/C, 10-Mo/C, and 15-Mo/C catalysts using NH_3-TPD.

Sample	Total acidity (mmol g^{-1})	Weak acid sites		Strong acid sites	
		Acidity (mmol g^{-1})	T_{max} (°C)	Acidity (mmol g^{-1})	T_{max} (°C)
C	0.9372	0.3716	220-230	0.5656	524
5-Mo/C	0.5440	0.1065	191-221	0.4375	525
10-Mo/C	0.7070	0.0872	175-221	0.6198	526
15-Mo/C	1.1472	0.0919	201-230	1.0553	571

The classification of acid site strength can be divided into weak acid sites, medium acid sites, and strong acid sites. Weak acid sites are formed at 150–300 °C, medium

acid sites are formed at 300–500 °C, and strong acid sites are formed at temperatures above 500 °C[48]. Based on Fig. 8, based on the NH_3-TPD analysis curve on 5-Mo/C, 10-Mo/C, and 15-Mo/C catalysts, two desorption peaks are formed. Desorption peaks in the region of 175 °C to above 200 °C indicate the presence of weak acid sites formed on the catalyst. The desorption peak formed at temperatures above 500 °C indicates the formation of strong acid sites on the catalyst. The peaks on Fig. 8 do not look clear enough because, during NH_3-TPD, the use of activated carbon as support should require a higher temperature during the degassing phase. The weak acid sites and strong acid sites formed on each catalyst will play a role in increasing the catalytic activity of the catalyst. Total acidity and acid sites are calculated using these equations as follows, where m and c are obtained from a straight-line equation using calibration data:

$$Total\ acidity = \frac{n_{NH3}}{W_{sample}} \quad (6)$$

$$Weak\ acid\ sites = m * A_{weak} + c \quad (7)$$

$$Strong\ acid\ sites = m * A_{strong} + c \quad (8)$$

Based on Table 6, the activated carbon has a greater total acidity than the catalyst after the addition of Mo metal, namely in the 5-Mo/C and 10-Mo/C catalysts. This occurred due to the uneven distribution of metal on the support, resulting in blockage by molybdenum and covering the acid sites contained on the catalyst, as seen in Fig. 4. The total acidity of the molybdenum-containing catalyst increases along with the increase in Mo metal composition. This indicates that Mo metal contributes acidity to the support, so that the acidity of the catalyst increases. Molybdenum acts as a contributor to Lewis acid sites because it has electrons in the unpaired *d* orbital, so it can act as an electron acceptor. The 15-Mo/C catalyst has the highest acidity among other catalysts, including activated carbon, due to the more even distribution of the Mo metal, which does not block the acid sites on the catalyst. This is also reinforced by the SEM imaging of 15-Mo/C in Fig. 4.

3.7 Catalytic Activity Test

Catalytic activity test by HDO reaction of RPKO result was shown in Table 7 and 8.

Table 7. HDO result of RPKO using activated carbon, 5-Mo/C, 10-Mo/C, and 15-Mo/C catalysts.

Catalyst	Yield (wt%)				
	Liquid product	Bioavtur	Oxygenated compounds	Non-bioavtur	Important bioavtur
Thermal	38.99	34.91	2.77	1.31	13.39
C	29.35	28.37	0.51	0.51	13.13
5-Mo/C	35.40	33.48	1.62	0.30	9.24
10-Mo/C	38.35	36.09	1.89	0.38	17.05
15-Mo/C	42.52	41.28	1.22	0	19.29

Based on Table 6, the activated carbon has greater total acidity than the catalyst after the addition of Mo metal, namely in the 5-Mo/C and 10-Mo/C catalysts due to the uneven distribution of metal on the support, resulting in blockage by molybdenum and covering the acid sites contained on the catalyst, as seen in Fig. 4. The total acidity of the molybdenum-containing catalyst increases along with the increase in Mo metal composition which indicates that Mo metal contributes acidity to the support, so that the acidity of the catalyst increases. Molybdenum acts as a contributor to Lewis acid sites because it has electrons in the unpaired *d* orbital, so it can act as an electron acceptor. The 15-Mo/C catalyst has the highest acidity among other catalysts, including activated carbon, due to the more even distribution of the Mo metal, which does not block the acid sites on the catalyst. This is also reinforced by the SEM imaging of 15-Mo/C in Fig. 4.

Non-bioavtur were hydrocarbons that were not in the C_7–C_{16} carbon range. For example, the bio-avtur compounds can be seen in Table 8 from n-heptane (C_7H_{16}) to n-hexadecane ($C_{16}H_{34}$), while non-bio-avtur compounds, for example, m-hexane (C_6H_{14}). Based on the data from Table 7, thermal cracking resulted in more liquid product than activated carbon (5-Mo/C and 10-Mo/C but had less bioavtur selectivity and produced more oxygenated and non-bioavtur compounds. The use of activated carbon as a catalyst without the presence of active metals showed the lowest conversion and bioavailability yield when compared to thermal cracking and catalysts containing molybdenum (Table 7). Although activated carbon had the lowest yield, it had a higher selectivity towards bioavtur than thermal cracking. This shows the catalyst support has a role in product selectivity, and activated carbon has carboxylic groups that can act as Bronsted acid sites, resulting in an increase in bioavailability.

The 15-Mo/C catalyst has the highest percentage of bioavtur yield, which can be explained by the acidity level of the catalyst. This shows that the 15-Mo/C catalyst has good activity and selectivity in the HDO reaction. This condition is supported by its high total acid site content and large pores, which can increase its ability to undergo HDO reactions. Based on the results of the acidity test with NH_3-TPD, it was found that the 15-Mo/C catalyst has the highest total acidity and contains the strongest acid sites. This can also be attributed to the decrease around the 15-Mo/C catalyst along with the increase in Mo metal concentration, which means that more active sites enter the pores and block the pores. The increase in pore diameter on the catalyst will make it easier for the catalyst to adsorb the feed, so the result will be higher yield and selectivity.

Table 8. Bioavtur compound distribution from HDO reaction with 15-Mo/C catalyst using GC-MS.

Retention time	Compound			Yield (wt%)		
	Name	SI	Formula	Lower fraction (400-500 °C)	Upper fraction (500-600 °C)	Total
3.68 – 3.84	1-heptene	96	C_7H_{14}	0.25	0.01	0.26
	n-heptane	95	C_7H_{16}	0.19	-	0.19
6.59 – 6.92	1-octene	96	C_8H_{16}	0.71	0.03	0.74
	n-octane	95	C_8H_{18}	0.49	0.01	0.51
10.61 – 10.96	1-nonene	97	C_9H_{18}	1.64	0.07	1.72
	n-nonane	96	C_9H_{20}	1.36	0.04	1.40
14.60 – 17.96	1-decene	96	$C_{10}H_{20}$	3.98	0.19	4.17
	Decane	97	$C_{10}H_{22}$	1.48	0.03	1.51
	2-decene	91	$C_{10}H_{20}$	0.46		0.46
	Cyclopentane, 1-isobutylidene-3-methyl-	90	$C_{10}H_{18}$	-	0.01	0.01
	2,6-dimethyl-Octene	82	$C_{10}H_{20}$	-	0.01	0.01
18.29 – 18.96	1-undecene	97	$C_{11}H_{22}$	6.70	0.26	6.96
	n-undecane	96	$C_{11}H_{24}$	9.09	-	9.09
	4-undecane	95	$C_{11}H_{22}$	-	0.01	0.01
	2-undecene	96	$C_{11}H_{22}$	0.30	0.28	0.57
21.57 – 21.96	1-dodecene	97	$C_{12}H_{24}$	2.64	0.08	2.71
	3-dodecene	90	$C_{12}H_{24}$	-	0.01	0.01
	n-dodecane	97	$C_{12}H_{26}$	1.61	0.04	1.66
	5-dodecene	87	$C_{12}H_{24}$	1.31	-	1.31
24.68 – 24.96	1-tridecene	96	$C_{13}H_{26}$	1.98	0.05	2.03
	n-tridecane	98	$C_{13}H_{28}$	3.77	0.10	3.87
27.54 – 27.76	5-tetradecene	94	$C_{14}H_{28}$	-	0.01	0.01
	1-tetradecene	98	$C_{14}H_{28}$	0.46	0.01	0.47
	n-tetradecane	97	-	0.25	-	0.25
	1-hexadecene	97	$C_{16}H_{32}$	0.52	-	0.52
	n-hexadecane	97	$C_{16}H_{34}$	0.81	0.02	0.83
Total yield (wt%)				40.00	1.28	41.28
Total yield (wt%) main avtur compound				19.02	0.26	19.28

Note * = Important avtur compound

According to a study by Benavides et al.[49], standard aviation gasoline samples' hydrocarbon component concentration exhibits a distribution of carbon atom counts ranging from C_7 to C_{19}. Table 8 shows the compound distribution of the 15-Mo/C catalyst biomass through GC-MS data. The GC-MS used a DB-5MS column with GC oven at 40 ºC. The liquid product contains hydrocarbons that are components of bioavtur from the same range as the C_7-C_{16} hydrocarbon range. The liquid product compounds were dominated by n-alkane and n-alkene compounds, both in the upper and lower fractions, and contained a total bioavtur yield of 40.00% with an important bioavtur content of 19.02%. To compare 15-Mo/C performance towards bioavtur conversion, a comparison was made and shown in Table 9.

Table 9. Comparison table between bioavtur production studies.

Catalyst	Feed	Reactor type	Condition	Bioavtur yield (wt%)	Reference
15-Mo/C	Palm kernel oil	Semi-batch with double furnace in one pot system	400-600 ºC, H_2 gas flow of 10 ml min^{-1}, 2 h	41.28	Present work
NiMo/Zeolit	Oleic acid	Autoclave batch	375 ºC, 1.48 atm, 2.5 h	36.32	[50]
Pd-SiO_2	Date seed oil	Autoclave batch	340 ºC, 150 rpm, 4 h	36.78	[51]
NiMo-2/SiO_2	Used cooking oil	Multilevel	425 ºC, 1% catalyst-to-feed ratio, H_2 gas flow of 20 ml min^{-1}, 2 h	39.48	[52]
4% MB	Jatropha oil	Batch	350-450 ºC, 18 min, 78.9 atm	40.00	[53]

In Table 9, oleic acid was transformed into bioavtur in a study by Carli et al. [50] using NiMo injected onto zeolite. A 2.5-hour autoclave batch reactor produced 36.32wt% of bioavtur. Jrai et al. converted date seed oil to bioavtur using Pd-SiO_2 made from recycled glass and wet-impregnated with palladium chloride, yielding 36.78wt% bioavtur in an autoclave batch reactor[51]. Agaradathu et al. used a multilevel reactor and a dual metal co-impregnation process with 2% of each Ni and Mo metal to create bioavtur from used cooking oil and produced 39.48wt% of bioavtur[52]. Jatropha oil was employed as the feed by Hassan et al., and Egyptian Bentonite B was used as the catalyst. A batch reactor operating at a high pressure of 78.9 atm produced 40% by weight of bioavtur[53]. The differences between the studies in Table 9 with 15-Mo/C performance are not using high pressure for HDO reactions like 4% MB, used less time than that of Carli et al. and Jrai et al., only using Mo metal with cheaper and more sustainable-renewable support and producing more bioavtur yield resulting in more efficient bioavtur yield.

3.8 Catalyst Usability Test

The result of 15-Mo/C catalyst usability test was shown in Table 10, Fig. 6, and Table 11.

Table 10. Liquid product and bioavtur yield after 15-Mo/C usability test by HDO of RPKO feed.

Run	Yield (wt%)					
	Liquid Product Fraction		Total	Bioavtur Fraction		Total
	Lower	Upper		Lower	Upper	
1	41.18	1.34	42.52	40.00	1.28	41.28
2	30.91	5.20	36.11	29.36	4.80	34.16
3	30.82	2.02	32.84	29.34	1.90	31.24

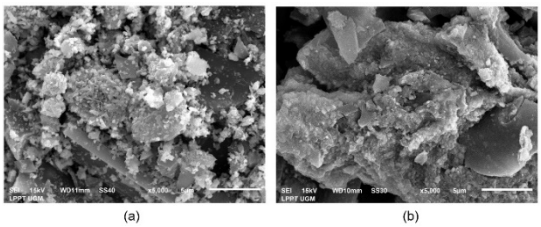

(a) (b)

Fig. 9: SEM imaging of: (a) 15-Mo/C catalyst and (b) 15-Mo/C catalyst after 3 HDO runs.

Table 11. Elemental Compositions of 15-Mo/C before and after usability test using EDX.

Element	Composition (wt%)	
	15-Mo/C	15-Mo/C after 3 HDO runs
Mo	29.75	4.66
C	47.50	55.03
O	21.91	20.64
K	0.26	-
Ca	0.57	0.62
Impurities	-	19.05

Repeated use of the 15-Mo/C catalyst has decreased liquid product and bioavtur as shown in Table 10. The second and third runs were similar, indicating promising catalytic performance and stability for multiple runs. The lower (400-500 °C) and upper fractions (500–600 °C) were separated to determine the best running temperature. As shown in Table 10, the lower fraction produced most of the yield, resulting in a more efficient conversion. The decrease in liquid product conversion can occur due to carbon deposits (coke) after each run. This explanation was reinforced by Fig. 9, where the blockage was caused by carbon deposits mixed with the remnants of RPKO that were not vaporized and trapped in the pores of the catalyst. The Mo composition in Table 11 decreased after 3 HDO runs due to metal leaching and clumping, which were caused by the coke. The Mo metal leaching happened maybe because the catalyst got into contact with the feed's vapor and left the catalyst surface. There is an increase in C composition after 3 HDO runs, which is the RPKO that was not vaporized during the HDO run.

4. Conclusion

The synthesis of HDO catalysts using spray-dry impregnation was successfully done and produced bioavtur from RPKO. Application of the synthesized catalyst to the HDO reaction of RPKO resulted in the best catalyst activity with the 15-Mo/C catalyst. The 15-Mo/C catalyst had the highest acidity among catalysts containing Mo metal at 1.1472 mmol g^{-1}, catalyst area of 12.31 m^2 g^{-1} and a pore diameter of 6.13 nm. The 15-Mo/C catalyst produced a liquid product conversion of 42.52wt% with bioavtur yield of 41.28wt%. The 5-Mo/C and 10-Mo/C catalysts produced liquid products of 35.40 and 38.35wt% with bioavtur yields of 33.48 and 36.09wt%, respectively. The 15-Mo/C catalyst had a promising performance during the second HDO run produced a liquid product of 36.11wt% and a bioavtur yield of 34.16wt% while the third run produced a liquid product conversion of 32.84wt% with a bioavtur yield of 31.24wt%.

Acknowledgement

This study was supported by Sawit Grant BPDPKS with grant numbers PRJ-365/DPKS/2022 and 3660/UN1/DITLIT/Dit-Lit/PT.01.03/2022.

Nomenclature

A_n	GC area of non-bioavtur compounds (%)
A_o	GC area of oxygenated compounds (%)
A_{peak}	XRD peak area (%)
A_{total}	Total GC, NH_3-TPD or XRD area (%)
A_{strong}	Strong acid sites area (>500 °C, %)
A_{weak}	Weak acid sites area (150-300 °C, %)
m	Line gradient
c	y-intercept
W_{LP}	HDO liquid product weight (g)

W_F RPKO feed weight (g)
Y_{BA} Bioavtur yield (wt%)
Y_{Nb} Non-bioavtur yield (wt%)
Y_{OC} Oxygenated compounds yield (wt%)

References

1) A. Gani, 'Fossil fuel energy and environmental performance in an extended stirpat model', *J. Clean. Prod.*, 297 (2021). doi:10.1016/j.jclepro.2021.126526.
2) S. Li, J. Meng, H. Zheng, N. Zhang, J. Huo, Y. Li, and D. Guan, 'The driving forces behind the change in energy consumption in developing countries', *Environ. Res. Lett.*, 16 (*5*) (2021). doi:10.1088/1748-9326/abde05.
3) H. Akamine, M. Mitsuhara, and M. Nishida, 'Developments of coal-fired power plants: microscopy study of fe-ni based heat-resistant alloy for efficiency improvement', *Evergreen*, 3 (*2*) 45–53 (2016). doi:10.5109/1800871.
4) A. Soemanto, E. Mohi, M.I. al Irsyad, and Y. Gunawan, 'The role of oil fuels on the energy transition toward net zero emissions in indonesia: a policy review', *Evergreen*, 10 (*4*) 2074–2083 (2023). doi:10.5109/7160867.
5) M.I. Sabtu, H. Hishamuddin, N. Saibani, and M.N. Ab Rahman, 'A review of environmental assessment and carbon management for integrated supply chain models', *Evergreen*, 8 (*3*) 628–641 (2021). doi:10.5109/4491655.
6) A.A.S. Gheidan, M.B.A. Wahid, O.A. Chukwunonso, and M.F. Yasin, 'Impact of internal combustion engine on energy supplyand its emission reduction via sustainable fuel source', *Evergreen*, 9 (*3*) 830–844 (2022).
7) H. Assad, S. Kaya, P. Senthil Kumar, D.V.N. Vo, A. Sharma, and A. Kumar, 'Insights into the role of nanotechnology on the performance of biofuel cells and the production of viable biofuels: a review', *Fuel*, 323 (2022). doi:10.1016/j.fuel.2022.124277.
8) L. Efiyanti, and D. Santi, 'The influence of nio and niomoo catalyst for hydrocracking of cashew nut shell liquid', *J. Penelit. Has. Hutan*, 34 (*3*) (2016).
9) M.A. Mohammad, 'Pengujian fixed bed gasifier dengan bahan bakar biomassa', *J. Tek. Mesin Indones.*, 14 (*1*) (2019). doi:10.36289/jtmi.v14i1.107.
10) H. Schobert, 'Chemistry of fossil fuels and biofuels', 2010. doi:10.1017/CBO9780511844188.
11) T. Güney, 'Renewable energy, non-renewable energy and sustainable development', *Int. J. Sustain. Dev. World Ecol.*, 26 (*5*) (2019). doi:10.1080/13504509.2019.1595214.
12) I. Khan, L. Han, H. Khan, and L.T. Kim Oanh, 'Analyzing renewable and nonrenewable energy sources for environmental quality: dynamic investigation in developing countries', *Math. Probl. Eng.*, 2021 (2021). doi:10.1155/2021/3399049.
13) S. Bhattacharjee, and C.S. Tan, 'Production of biojet fuel from octadecane and derivatives of castor oil using a bifunctional catalyst ni-pd@al-mcf in a pressurized co2-hexane-water solvent', *Energy and Fuels*, 36 (*6*) (2022). doi:10.1021/acs.energyfuels.1c03881.
14) W. Hunsiri, N. Chaihad, C. Ngamcharussrivichai, D.N. Tungasmita, P. Reubroycharoen, and N. Hinchiranan, 'Branched-chain biofuels derived from hydroisomerization of palm olein using ni/modified beta zeolite catalysts for biojet fuel production', *Fuel Process. Technol.*, 248 (2023). doi:10.1016/j.fuproc.2023.107825.
15) V. Itthibenchapong, A. Srifa, R. Kaewmeesri, P. Kidkhunthod, and K. Faungnawakij, 'Deoxygenation of palm kernel oil to jet fuel-like hydrocarbons using ni-mos2/γ-al2o3catalysts', *Energy Convers. Manag.*, 134 (2017). doi:10.1016/j.enconman.2016.12.034.
16) M. Makcharoen, A. Kaewchada, N. Akkarawatkhoosith, and A. Jaree, 'Biojet fuel production via deoxygenation of crude palm kernel oil using pt/c as catalyst in a continuous fixed bed reactor', *Energy Convers. Manag. X*, 12 (2021). doi:10.1016/j.ecmx.2021.100125.
17) B. Prastowo, 'Bahan bakar nabati asal tanaman perkebunan sebagai alternatif pengganti minyak tanah untuk rumah tangga', *Perspektif*, 6 (*1*) 10–18 (2015).
18) N.L. Sanusi, M.F. Ramadhani, N. Nurfadhlini, and L. Aisyah, 'Penentuan komposisi bahan bakar nabati dalam bahan bakar minyak campuran menggunakan metode direct counting c-14', *Eksplorium*, 42 (*2*) 149 (2021). doi:10.17146/eksplorium.2021.42.2.6363.
19) Y. Furutani, K. Norinaga, S. Kudo, J.I. Hayashi, and T. Watanabe, 'Current situation and future scope of biomass gasification in japan', *Evergreen*, 4 (*4*) 24–29 (2017). doi:10.5109/1929681.
20) J. Liao, Q. Zhong, J. Gu, S. Qiu, Q. Meng, Q. Zhang, and T. Wang, 'New approach for bio-jet fuels production by hydrodeoxygenation of higher alcohols derived from c-c coupling of bio-ethanol', *Appl. Energy*, 324 (2022). doi:10.1016/j.apenergy.2022.119843.
21) J. Silalahi, Lida Karo Karo, S.M. Sinaga, and Yosy Cinthya Eriwaty Silalahi, 'Composition of fatty acid and identification of lauric acid position in coconut and palm kernel oils', *Indones. J. Pharm. Clin. Res.*, 1 (*2*) 1–8 (2018). doi:10.32734/idjpcr.v1i2.605.
22) T. Dickerson, and J. Soria, 'Catalytic fast pyrolysis: a review', *Energies*, 6 (*1*) (2013). doi:10.3390/en6010514.
23) I. Barroso-Martín, D. Ballesteros-Plata, A. Infantes-Molina, M.O. Guerrero-Pérez, J. Santamaría-González, and E. Rodríguez-Castellón, 'An overview of catalysts for the hydrodeoxygenation reaction of model compounds from lignocellulosic biomass', *IET Renew. Power Gener.*, 16 (*14*) (2022).

doi:10.1049/rpg2.12477.
24) S. Oh, H. Hwang, H.S. Choi, and J.W. Choi, 'The effects of noble metal catalysts on the bio-oil quality during the hydrodeoxygenative upgrading process', *Fuel*, 153 (2015). doi:10.1016/j.fuel.2015.03.030.
25) J.G. Speight, 'Chapter 8 - The biorefinery', in: Biomass Process. Chem., 2022.
26) N. Arun, S. Nanda, Y. Hu, and A.K. Dalai, 'Hydrodeoxygenation of oleic acid using γ-al2o3 supported transition metallic catalyst systems: insight into the development of novel fecu/γ-al2o3 catalyst', *Mol. Catal.*, 523 (2022). doi:10.1016/j.mcat.2021.111526.
27) M. Žula, M. Grilc, and B. Likozar, 'Hydrocracking, hydrogenation and hydro-deoxygenation of fatty acids, esters and glycerides: mechanisms, kinetics and transport phenomena', *Chem. Eng. J.*, 444 136564 (2022). doi:10.1016/J.CEJ.2022.136564.
28) W. Wang, Y. Yang, H. Luo, H. Peng, B. He, and W. Liu, 'Preparation of ni(co)-w-b amorphous catalysts for cyclopentanone hydrodeoxygenation', *Catal. Commun.*, 12 (*14*) (2011). doi:10.1016/j.catcom.2011.04.027.
29) E.W. Qian, N. Chen, and S. Gong, 'Role of support in deoxygenation and isomerization of methyl stearate over nickel-molybdenum catalysts', *J. Mol. Catal. A Chem.*, 387 (2014). doi:10.1016/j.molcata.2014.02.031.
30) W. Trisunaryanti, I.I. Falah, D.R. Prihandini, and M.F. Marsuki, 'Synthesis of ni/mesoporous silica-alumina using sidoarjo mud and bovine bone gelatin template for hydrocracking of waste lubricant', *Rasayan J. Chem.*, 12 (*3*) (2019). doi:10.31788/RJC.2019.1235297.
31) K.D. Nugrahaningtyas, R.S.R. Suharbiansah, W.W. Lestari, and F. Rahmawati, 'Metal phase, electron density, textural properties, and catalytic activity of como based catalyst applied in hydrodeoxygenation of oleic acid', *Evergreen*, 9 (*2*) 283–291 (2022). doi:10.5109/4793665.
32) N.M. Wiratini, W. Trisunaryanti, and A. Kuncaka, 'Electrochemical removal of remazol black 5 (rb-5) using sio 2 / nio / ni nanocomposite electrocatalyst deposited on the surface of graphite electrodes', 10 (*03*) 1274–1285 (2023).
33) Y. Wibisono, A. Amanah, A. Sukoyo, F. Anugroho, and E. Kurniati, 'Activated carbon loaded mixed matrix membranes extracted from oil palm empty fruit bunches for vehicle exhaust gas adsorbers', *Evergreen*, 8 (*3*) 593–600 (2021). doi:10.5109/4491651.
34) A.F. Ridassepri, F. Rahmawati, K.R. Heliani, Chairunnisa, J. Miyawaki, and A.T. Wijayanta, 'Activated carbon from bagasse and its application for water vapor adsorption', *Evergreen*, 7 (*3*) 409–416 (2020). doi:10.5109/4068621.
35) F. Taufany, M.J. Pasaribu, B.Y.S. Romaji, Y. Rahmawati, A. Altway, Susianto, S. Nurkhamidah, J.G. Anfias, Y. Mursidah, D. Fujanita, S. Yulianti, D. Rahmawati, and G. Stellarosari, 'The synthesis of activated carbon from waste tyre as fuel cell catalyst support', *Evergreen*, 9 (*2*) 412–420 (2022). doi:10.5109/4794166.
36) N.C. Agustin, and R. Prasdiantika, 'Sintesis natrium zirkonia sebagai katalis reaksi transesterifikasi minyak goreng bekas', *J. Presipitasi Media Komun. Dan Pengemb. Tek. Lingkung.*, 17 (*1*) 44–51 (2020).
37) F.L. Rahayu, R. Nuryanto, and L. Suyati, 'Pengaruh diameter kanal pelet katalis zeolit aktif dan ni-zeolit terhadap pirolisis limbah batang pohon sagu (metroxylonsp.)', *J. Kim. Sains Dan Apl.*, 16 (*1*) 33 (2013). doi:10.14710/jksa.16.1.33-37.
38) P. Munnik, P.E. De Jongh, and K.P. De Jong, 'Recent developments in the synthesis of supported catalysts', *Chem. Rev.*, 115 (*14*) 6687–6718 (2015). doi:10.1021/cr500486u.
39) C. Guild, S. Biswas, Y. Meng, T. Jafari, A.M. Gaffney, and S.L. Suib, 'Perspectives of spray pyrolysis for facile synthesis of catalysts and thin films: an introduction and summary of recent directions', *Catal. Today*, 238 (2014). doi:10.1016/j.cattod.2014.03.056.
40) Y. Gao, W. Sun, W. Yang, and Q. Li, 'Creation of pd/al2o3 catalyst by a spray process for fixed bed reactors and its effective removal of aqueous bromate', *Sci. Rep.*, 7 (2017). doi:10.1038/srep41797.
41) I.A. Muna, F. Kurniawansyah, M. Mahfud, and A. Roesyadi, 'Synthesis and characterization of Cr-Co/γ-alumina catalyst for ethanol dehydration', in: AIP Conf. Proc., 2021. doi:10.1063/5.0052730.
42) R.P. Silvy, 'Scale-up of a nimop/γal2o3 catalyst for the hydrotreating and mild hydrocracking of heavy gasoil', *Oil Gas Sci. Technol.*, 74 (2019). doi:10.2516/ogst/2018094.
43) M. Khoshroo, and H. Hosseini-Monfared, 'Oxidation of sulfides with h2o2 catalyzed by impregnated graphene oxide with co–cu–zn doped fe3o4/co3o4–moo3 nanocomposite in acetonitrile', *J. Inorg. Organomet. Polym. Mater.*, 27 (*1*) (2017). doi:10.1007/s10904-016-0459-7.
44) S. Sharma, M. Kaur, C. Sharma, A. Choudhary, and S. Paul, 'Biomass-derived activated carbon-supported copper catalyst: an efficient heterogeneous magnetic catalyst for base-free chan-lam coupling and oxidations', *ACS Omega*, 6 (*30*) (2021). doi:10.1021/acsomega.1c01830.
45) S.A. Abdulhadi, and H.H. Alwan, 'Oxidative desulfurization of model fuel using a nio-moo3 catalyst supported by activated carbon: optimization study', *South African J. Chem. Eng.*, 43 (2023). doi:10.1016/j.sajce.2022.10.010.
46) M.Z. Hossain, M.B.I. Chowdhury, A.K. Jhawar, W.Z. Xu, M.C. Biesinger, and P.A. Charpentier, 'Continuous hydrothermal decarboxylation of fatty

acids and their derivatives into liquid hydrocarbons using mo/al2o3 catalyst', *ACS Omega*, 3 (*6*) (2018). doi:10.1021/acsomega.8b00562.

47) M.A. Sabri, G. Bharath, A. Hai, M.A. Haija, R.P. Nogueira, and F. Banat, 'Synthesis of molybdenum-cobalt nanoparticles decorated on date seed-derived activated carbon for the simultaneous electrochemical hydrogenation and oxidation of furfural into fuels', *Fuel Process. Technol.*, 238 (2022). doi:10.1016/j.fuproc.2022.107525.
48) S. Mosallanejad, B.Z. Dlugogorski, E.M. Kennedy, and M. Stockenhuber, 'On the chemistry of iron oxide supported on γ-alumina and silica catalysts', *ACS Omega*, 3 (*5*) (2018). doi:10.1021/acsomega.8b00201.
49) A. Benavides, P. Benjumea, F.B. Cortés, and M.A. Ruiz, 'Chemical composition and low-temperature fluidity properties of jet fuels', *Processes*, 9 (*7*) 1–13 (2021). doi:10.3390/pr9071184.
50) M.F. Carli, B.H. Susanto, and T.K. Habibie, 'Sythesis of bioavture through hydrodeoxygenation and catalytic cracking from oleic acid using NiMo/Zeolit catalyst', in: E3S Web Conf., 2018. doi:10.1051/e3sconf/20186702023.
51) A.A. Jrai, A.H. Al-Muhtaseb, F. Jamil, and M.T.Z. Myint, 'Green hydrocarbons fuel production from agricultural waste biomass in the presence of a novel heterogeneous catalyst', *Biomass Convers. Biorefinery*, (2023). doi:10.1007/s13399-023-04076-1.
52) R.H. Agharadatu, K. Wijaya, Prastyo, Wangsa, L. Hauli, and W.C. Oh, 'Application of mesoporous nimo/silica (nimo/sio2) as a catalyst in the hydrocracking of used cooking oil into jet fuel', *Silicon*, (*0123456789*) (2023). doi:10.1007/s12633-023-02683-1.
53) S.H. Hassan, N.K. Attia, G.I. El Diwani, S.K. Amin, R.S. Ettouney, and M.A. El-Rifai, 'Catalytic hydrocracking of jatropha oil over natural clay for bio-jet fuel production', *Sci. Rep.*, 13 (*1*) 1–11 (2023). doi:10.1038/s41598-023-40500-2.